Macromolecules

Article

pubs.acs.org/Macromolecules

Computational Study of the Structure and Rheological Properties of Self-Associating Polymer Networks

Mark Wilson,[†] Avinoam Rabinovitch,[§] and Arlette R. C. Baljon*[,‡]

[†]Department of Computational Science and [‡]Department of Physics, San Diego State University, San Diego, California 92182, United States

[§]Department of Physics, Ben-Gurion University of the Negev, Beer Sheva, Israel

Supporting Information

ABSTRACT: Utilizing a novel, hybrid molecular dynamics, Monte Carlo simulation, we report on microstructural changes in a polymer network that arise in response to oscillatory shear deformation. We model telechelic self-associating polymers as a course-grained, bead−spring system. The stress response of the system is obtained from rheological experiments and is reported as a function of frequency and amplitude in both the linear and nonlinear regimes. The frequency-dependent material properties are then correlated with observed changes in the topological network structure. While only minimal structural variations are observed in the elastic regime, a substantial rearrangement occurs in the low frequency, large amplitude viscous regime. Aggregates tend to break apart, resulting in an increased density of free chains. Additionally, the network tends to break and form larger structural elements with an increase multiplicity of chains bridging between the same two aggregates.

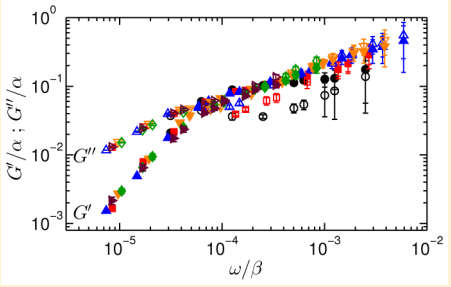

INTRODUCTION

Associating polymers have the unique ability to span a large spectrum of rheological properties, from fluid-like viscosity to near solid-like elastic dynamics. Telechelic polymers are one class of associating polymers. These triblock polymers consist of two differing chemical groups. The backbone has a high molecular weight and is constructed from multiple, repeating units. The two functionalized ends of the molecule, referred to as end groups, are members of a different chemical group and comprise a small fraction of the total molecular weight. In solution, end groups tend to aggregate by gathering into localized domains. At low enough temperatures and at concentrations above the micelle transition, a space spanning network is formed. The nodes of this network consist of aggregates of end groups, while links between aggregates are formed by one or more bridging polymer chains. End groups associate and dissociate from aggregates frequently; therefore, the topological structure within the network exhibits transient behavior.

The general fluid thickening characteristics of telechelic polymers have long since had utility as a rheological modifier in industrial applications within coatings[1] such as paints, adhesives, plastics, and sealants. Over the past few decades, they have come into considerable interest in a multitude of fields. Most recently, composite materials, partially composed of telechelic polymers, have found their respective place in medical and biological applications. Examples include a temporary matrix for bone tissue regeneration[2] and an injectable drug delivery method[3,4] along with regenerative tissue engineering for wound dressing.[5] Within these applications a water-soluble polymer is desirable, constructed as a hydrophilic backbone terminated by hydrophobic groups.[6−9] Because of the fact that these materials are primarily water by weight, they can exhibit biocompatible and biodegradable properties. They can also be subject to external parameters such as temperature and pH.[10,11] The behavior of these materials is highly sensitive to their chemical composition, allowing experimentalists to readily tune material properties, broadening the number of potential applications.

Understanding and quantifying the characteristics that lead to observed rheological properties is crucial to optimally design materials. These properties have origins in the structural content of the polymer network and in the dynamics of the formation and breakup of aggregates. The following article contains a computational study, wherein the transient structure within the polymer network is investigated throughout the viscoelastic regime. A novel molecular dynamics simulation of telechelic polymers is utilized.[12] We perform rheology experiments by imposing oscillatory strain and focus on identifying microstructural deviations in topology as a stress response.

METHODS

We designed and utilize a hybrid molecular dynamic (MD), Monte Carlo (MC) simulation of telechelic polymers. The computational simulation is based on the framework established by Kremer and Grest.[13] Polymer chains are modeled in course-grained fashion as a string of beads connected by springs. Each bead corresponds to multiple

Received: April 28, 2015
Revised: July 16, 2015
Published: August 20, 2015

DOI: 10.1021/acs.macromol.5b00885
Macromolecules 2015, 48, 6313−6320

monomer units within an atomistic representation. The imposed forces between beads are modeled through potential energy interactions. Our simulation utilizes two different pairwise potentials. The first is a shifted and truncated Lennard-Jones (LJ) potential which provides excluded volume interactions between beads

$$U_{LJ}(r_{ij}) = \begin{cases} 4\epsilon\left[\left(\frac{\sigma}{r_{ij}}\right)^{12} - \left(\frac{\sigma}{r_{ij}}\right)^{6} - \left(\frac{\sigma}{r_c}\right)^{12} + \left(\frac{\sigma}{r_c}\right)^{6}\right] & \text{for } r_{ij} \le r_c \\ 0 & \text{for } r_{ij} > r_c \end{cases} \quad (1)$$

The variable $r_{ij} = |\vec{r_i} - \vec{r_j}|$ is the Euclidean distance between two beads i and j. All beads in the model interact with each other through this potential. A cutoff distance of $r_c = 2^{1/6}\sigma$ is used to speed up the interaction calculations within the simulation.[14] All units within reported results are in terms of reduced LJ parameters: length σ, energy ϵ, and time $(m\sigma^2/\epsilon)^{1/2}$, with the bead mass $m = 1$. The parameter σ is a measure for the diameter of a bead. Temperature is measured in units of ϵ/k_b.

Each polymer is constructed as a chain of eight beads in length. The chain structure is maintained numerically throughout the simulation, such that nearest-neighbor beads along the chain are permanently bonded through an anharmonic, finitely extensible, nonlinear, elastic (FENE) potential

$$U_{FENE}(r_{ij}) = -\frac{1}{2}\kappa {R_0}^2 \ln\left[1 - \left(\frac{r_{ij}}{R_0}\right)^2\right] \quad (2)$$

for $r_{ij} < R_0$. The FENE potential diverges logarithmically as $r_{ij} \to R_0$. This provides a finite distance between chain beads. An appropriate choice of parameter values $R_0 = 1.5$ and $\kappa = 30.0$ prevents the possibility of chains passing through one another.[15]

The experimental system is composed of 1000 polymer chains and is contained within a simulation cell of dimensions 23.70 × 20.52 × 27.84. Periodic boundary conditions are employed in the horizontal directions, while solid surfaces confine the simulation in the vertical direction. Each of the two solid surfaces is constructed as a collection of 400 beads with a diameter of 0.8, distributed spatially over a two layer face-centered cubic lattice. A repulsive LJ interaction is applied between polymer beads and surface beads. Five percent of the total simulated polymer chains are permanently grafted to the surfaces by one end group to prevent wall slip during rheological experiments. Twenty-five beads are attached to the upper surface and 25 to the lower surface, all at an even spacing. The grafting is accomplished numerically by assigning a permanent FENE interaction between the grafted end group and a specified bead within the surface. Because of the smaller radius of the surface beads, $R_0 = 1.35$ and $\kappa = 37.0$ for interactions between surface and fluid beads.

Molecular dynamics governs the time-dependent positions of beads within the simulation. The positions are updated in three dimensions by integrating the equations of motion using a fifth-order Gear predictor−corrector algorithm[16] with a time step of 0.005. The temperature is controlled by coupling the simulation cell to a heat bath according to the fluctuation dissipation theorem as described by Kremer et al.[13]

The beads at each of the chain ends represent functionalized groups. To model the associative properties of these groups, we use a discrete MC step to form reversible, physical bonds. Each end group can have bonds with multiple other end groups. These bonds are modeled by a FENE potential with the same parameters as that of the intrachain bonds, to which a negative constant U_{ASSOC} is added. The association energy U_{ASSOC} can be considered a bond formation affinity. The parameter's magnitude affects the overall dynamics within the simulation, defining the temperature at which aggregation and ultimately dynamical arrest occurs. We choose $U_{ASSOC} = -22$, setting a convenient temperature range, spanning fluid-like dynamics at the highest temperatures the simulation can reach and dynamic arrest at the lowest temperatures.[12] The formation and breaking of these reversible bonds take place according to a Metropolis algorithm.[17] The MC step is as follows. Every 20 MD steps an attempt is made to change the bonded state between each end group. The state is switched if the difference between the current and the proposed configuration results in a decrease in energy $\Delta U < 0$. In the case where $\Delta U > 0$, the bonded state is switched with a probability according to a Boltzmann factor $e^{-\Delta U/k_bT}$. This algorithm will tend to switch bonding configurations more often at high temperatures than at low ones. Shearing the system tends to break bonds. As shear forces are imposed, the bonds between end groups become stretched. Since stretched bonds have a higher energy, the algorithm will favor breaking them, resulting in a decrease in energy. More frequent bond configuration updates did not statistically change the results of simulations discussed in this article. Our technique differs from that employed by others,[18] who gave the end groups a greater affinity to each other than to all other groups. The method at hand has the advantage that it can explicitly track which end groups are connected to each other.

In an earlier article,[12] characteristic temperatures were identified wherein the MD simulation undergoes structural changes. These lead to a fluid to gel-like transition in dynamics when the temperature was lowered. The relaxation time was determined according to Stokes−Einstein theory and provided insight into these characteristic temperatures and structural transitions. The relaxation time was shown to obey Arrhenius behavior in the high temperature range, indicating fluid-like dynamics. The system contained free chains which were infrequently bonded to other end groups. At the lower temperatures, Vogel−Fulcher theory predicted an extrapolated divergence of the relaxation time at $T = 0.29$. This temperature marked dynamic arrest, wherein the diffusivity of polymer chains goes to zero and the viscosity becomes infinite. The crossover between Arrhenius to diverging toward dynamic arrest occurred at $T = 0.75$. Structurally, this was the onset of a dramatic increase in the number of bonds Φ within the system. The micelle transition, occurring at $T = 0.51$, was identified where $\delta^2\Phi/\delta T^2 = 0$. This structural transition was accompanied by a peak in the specific heat. Geometrical percolation was found to occur at $T = 1.5$, even though the system acts as a fluid and not a gel at this high temperature. This provided evidence that gelation does not necessarily coincide with percolation. In fact, percolation tends to precede gelation due to the transient nature of the bonds within the polymeric network. Gelation at lower temperatures is a result of bonds having a longer lifetime. Therefore, structural components are maintained for longer durations.

RHEOLOGICAL PROPERTIES

Rheological experiments were performed by imposing a sinusoidal strain $\gamma(\tau) = \gamma_0 \sin(\omega\tau)$ (Figure 1a) to the upper

DOI: 10.1021/acs.macromol.5b00885
Macromolecules 2015, 48, 6313−6320

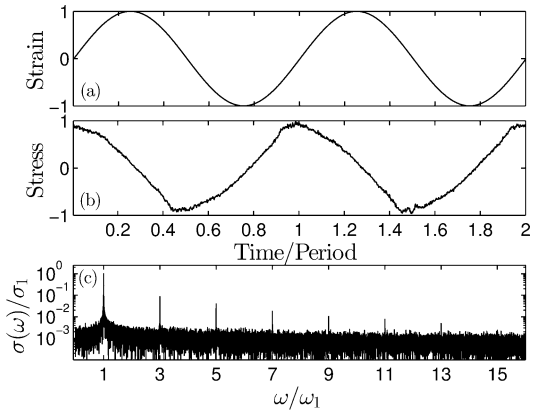

Figure 1. Time series of (a) the input normalized strain $\gamma(\tau)/\gamma_0$ and (b) the normalized stress $\sigma(\tau)/\sigma_{max}$ response waveform. The stress response data have been averaged over multiple periods of oscillation. (c) Frequency dependence of the relative intensities $\sigma(\omega)/\sigma_1$ of the harmonic contributions, where ω_1 is the input strain frequency and σ_1 is the magnitude of the first harmonic.

surface of the simulation cell while holding the lower surface at a constant position. A two parameter space was explored, varying amplitude γ_0 and frequency ω of the applied oscillatory strain independently. All numerical experiments were started from an identical, well-equilibrated, initial configuration at a temperature of $T = 0.4$. The force F on the top surface of the simulation cell, necessary to maintain the sinusoidal motion, was traced over time. The stress response $\sigma(\tau)$ (Figure 1b) was then calculated as $\sigma = F/A$, where A is the cross-sectional area of the simulation cell in the xy-plane. This discrete time series displayed a distorted, time-lagged waveform which was then characterized according to a Fourier series

$$\sigma(\tau, \gamma_0, \omega) = \gamma_0 \sum_n [G'_n(\tau, \gamma_0, \omega) \sin(n\omega\tau) + G''_n(\tau, \gamma_0, \omega) \cos(n\omega\tau)] \quad (3)$$

The viscoelastic properties of materials are typically reported in terms of the primary harmonic of this Fourier series. These values describe the leading order behavior and are attributed to a linear stress response. We follow convention and refer to the primary harmonic (G'_1 and G''_1) as the storage and loss moduli, denoted as G' and G'', respectively. Equation 3 can be rewritten in terms of the harmonic intensity σ_n and phase angle δ_n

$$\sigma(\tau, \gamma_0, \omega) = \sum_n \sigma_n(\tau, \gamma_0, \omega) \sin[n\omega\tau + \delta_n(\tau, \gamma_0, \omega)] \quad (4)$$

The frequency dependence of the relative intensities $\sigma(\omega)/\sigma_1$ of the harmonic contributions (Figure 1c) is shown to be primarily odd, with the magnitude decreasing with increasing harmonic number. The stress response of viscoelastic materials is typically independent of the direction of applied shear.[19] This symmetry leads to the dominance of odd harmonics.

The moduli were determined at each period of oscillation. We report these values as an average over multiple periods, taken after transient effects such as time-dependent moduli have subsided. Figure 2 shows the strain amplitude dependence of the moduli for several frequencies of oscillation. Error bars indicate the standard deviation. In the low amplitude range the moduli are observed to be independent of strain amplitude. This corresponds to a linear stress response which is primarily

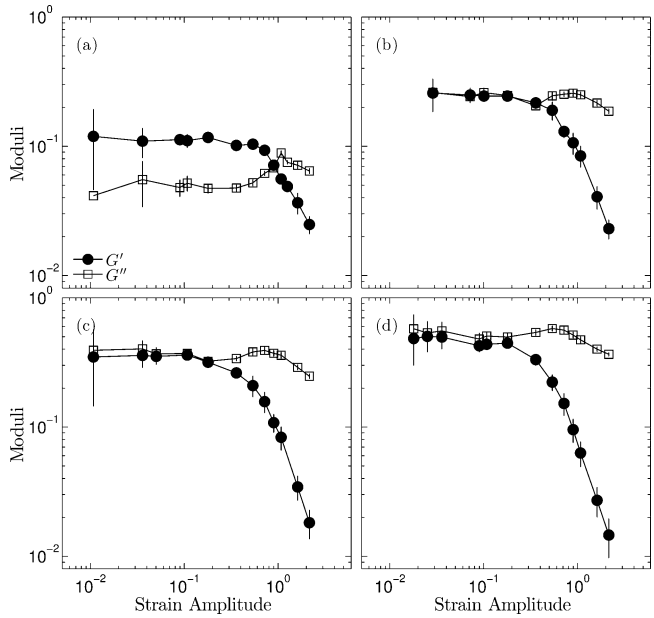

Figure 2. Strain amplitude dependence of the storage and loss moduli for several angular frequencies of oscillation: (a) 5.03×10^{-4} rad/τ, (b) 6.28×10^{-3} rad/τ, (c) 1.26×10^{-2} rad/τ, (d) 2.51×10^{-2} rad/τ. Data are reported as average values over multiple periods of oscillation. Error bars report the standard deviation in this data. Lines are shown as guides to the eye.

elastic ($G' > G''$) at the lowest frequency (a), crossing over to viscous at larger frequencies (b–d). The system exhibits a stress thinning behavior with increased amplitude. Both G' and G'' decrease, with the storage modulus dropping off faster than the loss modulus. A weak stress overshoot is observed as a local maximum in the loss moduli at medium amplitudes. The transition to amplitude dependent moduli is a hallmark sign of a nonlinear material response. This behavior is accompanied by the onset of a distorted stress waveform and, as a result, the development of higher order harmonics within the moduli. A measure of the nonlinear contributions in terms of the Fourier series is the intensity of the third harmonic relative to the first σ_3/σ_1 (not shown here). Although our system exhibits the characteristic indicators of nonlinearities, we find that it only has small nonlinear contributions from this measure. Over the range of amplitudes and frequencies reported, σ_3/σ_1 reaches a maximum value of 0.15.

The frequency dependence of the moduli within experimental telechelic systems are known to be well-described by a single Maxwellian model.[20] At low frequencies the moduli are within a viscous regime, where $G' < G''$. This viscous behavior typically exhibits a frequency dependence which scales as $G' \propto \omega^2$ and $G'' \propto \omega$. With increased frequency the moduli tend toward $G' = G''$ identifying a crossover from the viscous regime to the elastic plateau regime ($G' > G''$) at even higher frequencies. The crossover marks a structural relaxation time scale $\tau_s = 1/\omega_c$ transitioning from dissipative flow at long time scales to elastic response at shorter scales.

Figure 3 shows log–log plots of the frequency dependence of the moduli at constant strain amplitudes. At the smallest amplitude (a), the system is in the linear regime. The elastic plateau regime is observed at lowest frequencies reported. We do not observe the linear viscous response within our experiments. The predominant elastic response at these frequencies is explained in that the system lacks sufficient

DOI: 10.1021/acs.macromol.5b00885
Macromolecules 2015, 48, 6313–6320

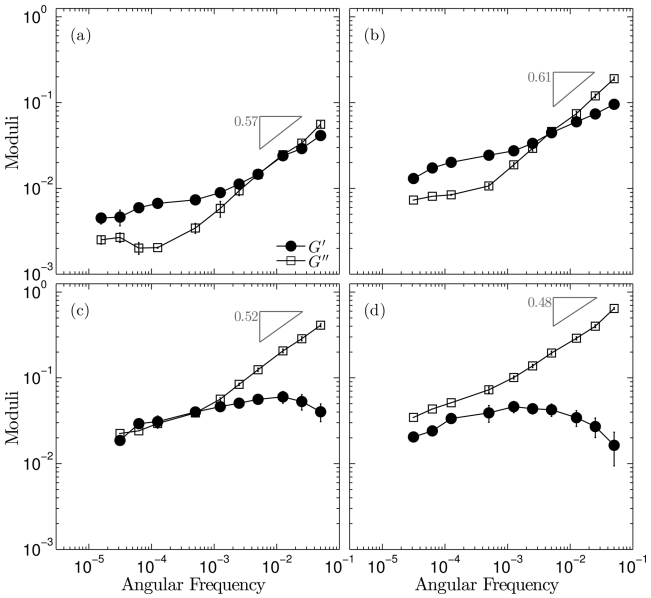

Figure 3. Frequency dependence of the storage (filled symbols) and loss moduli (open symbols) for several strain amplitudes: (a) 0.108, (b) 0.359, (c) 0.898, and (d) 1.616. Data are reported as average values over multiple periods of oscillation. Error bars report the standard deviation in this data. Lines are shown as guides to the eye.

time to rearrange the network structure. Energy is mainly stored elastically in the stretching of bridging polymer chains. We have verified that the end-to-end distance of chains indeed reaches a maximum at the extrema of the oscillatory strain period within this elastic regime.

In our earlier work,[12] a relaxation time for the system was obtained from diffusion at rest measurements using a Vogel–Fulcher fit. A relaxation time of $\tau \approx 10^4$ was determined, indicating we should expect the crossover ω_c to occur around $\omega = 2\pi f \approx 10^{-4}$. However, we do not observe it within our data. We noted in the previous work that other fits to relaxation data can be used instead of Vogel–Fulcher, which give longer relaxation times for this data. Our rheological results are validated in that the expected crossover of the moduli would fall at a frequency lower than 10^{-4} and would not necessarily be observed within the data presented here. It is extremely difficult to investigate even lower frequencies ($\omega \leq 10^{-5}$) within MD bulk rheology, simply due to the computational time. Several periods of oscillation are typically desired to obtain statistically accurate results. It is not practical to obtain these results in a reasonable quantity of time.

The moduli tend toward $G' = G''$ at high frequencies, where a near $\omega^{1/2}$ dependence in G'' is observed for all amplitudes. This behavior is predicted by Rouse-type dynamics[21] and can be attributed to frictional dissipation of Brownian particles. With increasing amplitude, the low frequency response tends to become dissipative (Figure 3c,d). A maximum in G' is observed in the largest amplitude data. Since elastic behavior is dependent upon the existence of bridging chains, a decrease in the elastic response suggests a decrease in network connectivity. This trending behavior can be attributed to the fact that these larger amplitudes cannot be reached without physically pulling the network apart. Large amplitudes and high frequencies do not allow for sufficient time for the system to relax and therefore self-assemble. This results in a decrease in the number of elastically active chains and as a consequence a decrease in G'. Snapshots of the simulation cell (not shown) provided evidence of this connectivity loss with a type of fracture being exhibited at the highest frequencies.

Strain Rate–Frequency Superposition. The rheological results presented earlier are typical of soft materials. We adopt the method employed by Wyss et al.[22] on other soft materials to investigate further modes of relaxation. The approach is to explore the frequency and amplitude parameters simultaneously, while maintaining constant strain rate amplitude $\dot{\gamma} = \gamma_0\omega$. The moduli are determined through bulk rheology over a range of frequencies for one $\dot{\gamma}$. At each given frequency, the amplitude is determined so as to hold $\dot{\gamma}$ constant. As a result, low frequency data correspond to large amplitudes and high frequencies to small amplitudes. The procedure is performed for multiple strain rates. If similar dynamics and relaxation processes exist throughout the oscillatory period for each strain rate, then there will be an observed consistency in the overall behavior of the moduli. Consequently, an appropriate choice of scaling factors should result in a collapse of the moduli data onto a single master curve. The procedure is referred to as "strain rate–frequency superposition" (SRFS). Wyss et al. showed that a scaling of the moduli in the frequency domain resulted in a data collapse for a wide variety of soft materials including a hydrogel suspension, a PMMA hard-sphere colloid, foam, and an oil emulsion.

We start by looking at the unscaled rheological response of the simulated system shown in Figure 4 for several strain rates.

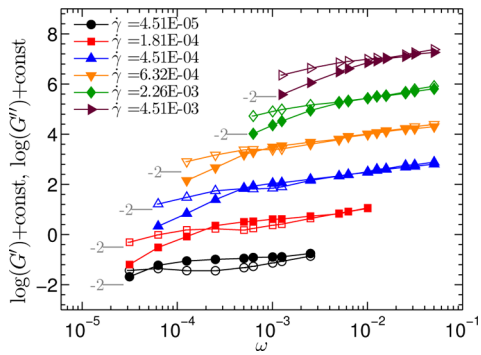

Figure 4. Storage (filled symbols) and loss moduli (open symbols) for the simulated system, obtained by maintaining a constant strain rate throughout the frequency sweep. Data are shown for several strain rates. Each data set is shifted in the vertical direction by a constant multiple for clarity. The ordinate scale is reported for data at $\dot{\gamma} = 4.51 \times 10^{-5}$, and a value of −2 is indicated for each respective data set. Lines are shown for guides to the eye.

The increased amplitude in the low frequency range forces the crossover to higher frequencies with increased shear rate. A low frequency viscous regime is now visible as a nonlinear response. The elastic plateau regime becomes shorter in length of frequency range with increased strain rate. At the highest shear rate an elastic region can no longer be observed.

Figure 5 shows the scaled moduli G'/α and G''/α as a function of scaled frequency ω/β. The inset shows the magnitude of these scaling factors α and β for multiple strain rates. The storage moduli scale well over the entire frequency range, whereas the loss moduli only scale in the lower frequency regime. Variations in the frequency length of the elastic plateau regime gives rise to the region where the loss moduli do not scale well. A frequency dependence of $G' \propto \omega^{1.86}$ and $G'' \propto \omega^{0.91}$ is observed. It is important to note that the low

DOI: 10.1021/acs.macromol.5b00885
Macromolecules 2015, 48, 6313–6320

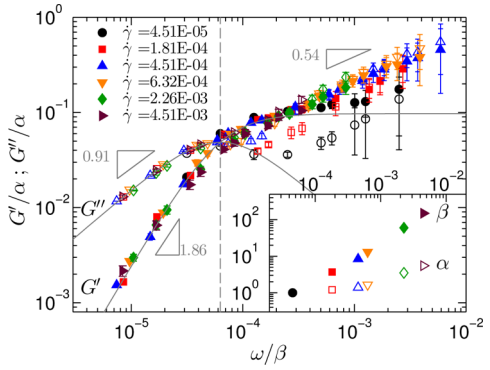

Figure 5. Frequency dependence of the storage and loss moduli, scaled to overlay the data from several constant strain rates $\dot{\gamma}$. Data are reported as average values over multiple periods of oscillation. Error bars report the standard deviation in this data. Inset shows the magnitude of the scaling parameters α and β as a function of strain rate.

frequency regime corresponds to the largest amplitudes within SRFS. We have already shown that large amplitudes result in an increase in nonlinear behavior. Therefore, the viscous regime has the largest nonlinearities. The exponents of the frequency dependence maintain a ratio of nearly 2:1, although their magnitudes are not 2 and 1, as would be expected in the linear regime. The dashed line marks a scaled crossover frequency ω_c/β, determined from a fit of a single relaxation Maxwell model (solid lines) in the low frequency range. The crossover frequency was determined to be $\omega_c/\beta = 6.3 \times 10^{-5}$, resulting in a structural relaxation time of $\tau_s = 1.6 \times 10^4$. We note that the value of τ_s is dependent upon the choice of $\dot{\gamma}$ wherein the scaling factor $\beta = 1$. Therefore, correlations between τ_s and earlier reported relaxation times[12] cannot be made.

Wyss et al. showed, in their data, that the failure of scaling in the loss moduli at large ω was due to an additional Rouse contribution. By removing this contribution such that $G'' = G''(\omega) - c\omega^{1/2}$, solely the local maximum near the crossover frequency remained and the data collapse nicely. Figure S1 of the Supporting Information shows that we can obtain a similar result for our data. This indicates that the structural relaxation contributions to the loss moduli are consistent for the strain rates and frequencies explored herein.

Nonlinearities. One method to investigate the nonlinear contributions to the stress response waveform is in the overall magnitude of σ_3/σ_1. A second method, which supplies substantially more information, is a plot of $\sigma(\gamma)$, obtained from $\sigma(\tau)$ and $\gamma(\tau)$. These plots are commonly referred to as Lissajous trajectory curves. They provide insight into the phase difference between the stress response and the strain along with the linearity of the response waveform. The phase of the first harmonic δ_1 (eq 4) provides the general shape of the trajectory and identifies viscous or elastic type behavior of the system. An oval trajectory is observed in the viscous regime, where the stress is out of phase with the applied strain ($\delta_1 = \pi/2$). Viscoelastic responses have phase angles ranging from $0 \leq \delta_1 \leq \pi/2$ and have elliptical trajectories. A purely elastic stress response is in phase with the strain ($\delta_1 = 0$) and is observed as straight line trajectory. Nonlinear contributions are associated with the onset of increased amplitude of higher order harmonics within the response. These contributions can be observed as a deviation from a perfectly sinusoidal stress waveform and, as a consequence, a deviation from the three trajectories mentioned above. Figure 6 shows Lissajous trajectory curves for the simulated system, organized in a space of increasing strain rate and angular frequency. Each trajectory reports normalized stress $\sigma(\tau)/\sigma_{max}$ versus normalized strain $\gamma(\tau)/\gamma_{max}$ shown in black. These trajectories are averaged over multiple periods of oscillation. The dashed blue trajectory is the linear contribution to the stress response and is determined from the inverse Fourier transform of the primary harmonic of the stress response. Variations between the two trajectories are nonlinear contributions to the response, arising from the third and higher harmonic contributions. The background color to each pane indicates the magnitude of the σ_3/σ_1 measure of nonlinearity. The number in the center of

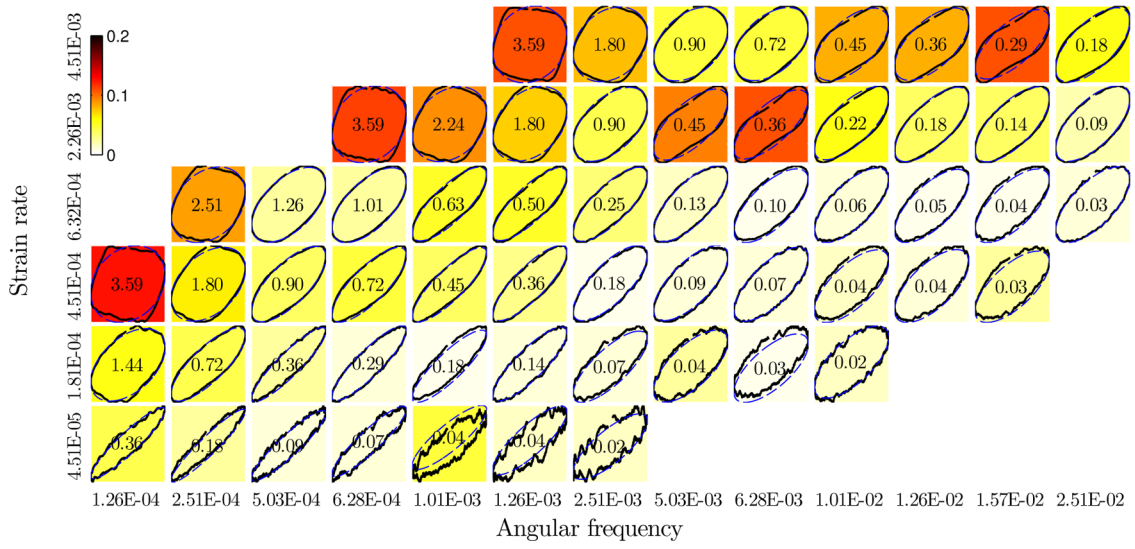

Figure 6. Lissajous trajectory curves organized in a space of strain rate and angular frequency. Each trajectory, shown in black, reports the normalized average stress as a function of normalized strain. The linear response, overlaid as a dashed blue line, is constructed from the first harmonic of the stress response. Numbering indicates the strain amplitude for the given strain rate−frequency combination. Coloring of each pane reports the intensity of the third harmonic over the first σ_3/σ_1, a measure of the nonlinearity of the stress response.

DOI: 10.1021/acs.macromol.5b00885
Macromolecules 2015, 48, 6313−6320

each pane indicates the strain amplitude for the given angular frequency and strain rate combination.

Recently, Hyun et al.[19] showed that the shape of the nonlinear contributions to the waveform can be described through the relative phase of the third harmonic δ_3' to the first, such that $\delta_3' = \delta_3 - 3\delta_1$. Applying a shift in time $\tau = \tau' - \delta_1'/\omega$ and expanding eq 4 to $n = 3$, we find

$$\sigma(\tau') = \sigma_1 \sin(\omega\tau') + \sigma_3 \sin(3\omega\tau' + \delta_3') \quad (5)$$

The authors explored the corresponding waveform over a range $0 \leq \delta_3' \leq 3\pi/2$ in the viscoelastic regime ($\delta_1 = \pi/4$). The Lissajous trajectories within our data (Figure 6) at $\dot{\gamma} = 4.51 \times 10^{-3}$ show evidence of the majority of this δ_3' range. A phase angle of $\delta_3' = 3\pi/4$ produces a stress waveform with a "forward tilted shoulder". That is to say, the stress overshoots, early in time, relative to a sinusoid with the same phase. An example of this waveform can be observed in Figure 1b, and the resultant trajectory is shown at a frequency $\omega = 1.26 \times 10^{-3}$. A triangular waveform occurs at a phase angle $\delta_3' = \pi/2$. A representative trajectory is observed at $\omega = 5.03 \times 10^{-3}$. A "backward tilted shoulder" is the outcome of $\delta_3' = \pi/4$. Here, the stress overshoots, late in time, relative to the same phase sinusoid. This shape trajectory is observed at $\omega = 1.57 \times 10^{-2}$. As δ_3' tends toward zero, the corresponding waveform transitions to rectangular. Our data do not explore this waveform.

The largest nonlinear contributions occur within trajectories that are consistent with the $\delta_3' = 3\pi/4$ and $\delta_3' = \pi/4$ waveforms. The $\delta_3' = 3\pi/4$ trajectory is a viscous response. This increase in nonlinearity is expected due to the larger amplitude of oscillation. Interestingly, as frequency increases, the four highest strain rates exhibit a local minimum and subsequent maximum in nonlinearity, before reaching the highest frequencies. This maximum is associated with the $\delta_3' = \pi/4$ trajectory and occurs near the unscaled crossover frequency. Nearly linear viscoelastic trajectories are observed within the highest frequencies of the Lissajous space.

STRUCTURAL PROPERTIES

A characterization of structural features within the polymer network is focused around aggregates and the connecting chains, bridging between these aggregates (Figure 7). Aggregates are identified by their size, the number of connected end groups. The presence of FENE bonds is used to identify which end groups belong to a given aggregate. The simulation allows for each end group to be reversibly bonded with multiple

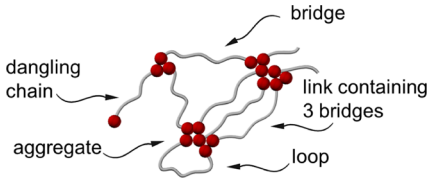

Figure 7. Cartoon of the structural elements found within a polymer network. Chain beads are not shown within the figure for clarity. Aggregates are collections of polymer chain end groups (shown as red beads). Loops are chains with both end groups within the same aggregate. Bridges have their end groups in two different aggregates. More than one chain can connect the same two aggregates. We call this type of connection a link, while the number of chains is referred to as its weight. Dangling chains have only one end group with a connection. Note that all simulations are performed in three dimensions.

other end groups. Hence, the end groups contained within a single aggregate will have a connected path of FENE bonds, physically joining them together. The end groups of a polymer chain can be contained either within a single aggregate or within two different aggregates. These two types of chains are referred to as a loop or a bridge, respectively. One or multiple bridges that connect the same two aggregates form links. The weight of a link is the number of chains it contains. Hence, the number of bridging chains equals the number of links multiplied by their average weight.

Figure 8 shows the frequency dependence of the number of aggregates and the loop to bridge ratio. Data are reported as

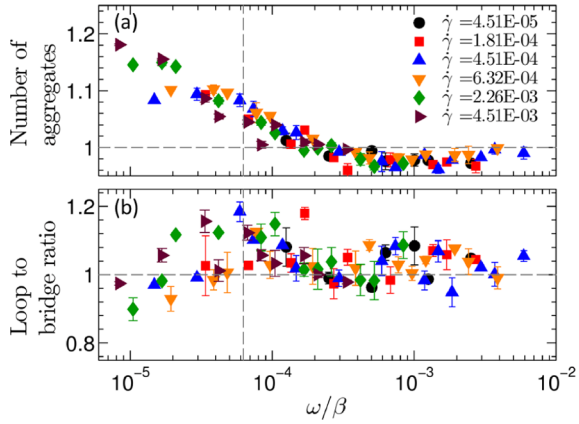

Figure 8. Frequency dependence of structural content within the polymer network. The top pane shows the number of aggregates, while the lower pane indicates the loop to bridge ratio. Data are reported for several strain rates as time averaged values. Error bars report the standard deviation in the data. Data have been normalized by the quantity of structural features found within a nonsheared system.

time averages of the given feature, starting from a time where initial transient effects have subsided. The data have been normalized by the quantity of the same structural feature found within a nonsheared system. Data greater than a value of one indicate an increase in the given feature due to the application of oscillatory strain. Data for the total number of aggregates, shown in Figure 8a, indicate a clear trend. Moreover, they appear to scale with the same factor β that collapses the moduli. The scaled crossover frequency ω_c/β is shown as a vertical dashed line. Below the crossover frequency the number of aggregates increases when the frequency decreases. This is expected in that low frequencies correspond to larger amplitudes, which cannot physically be reached without a significant restructuring of the polymer network. Aggregates are being pulled apart, and this results in more smaller sized aggregates. To further explore this restructuring, we obtained the aggregate size distribution (Figure 9). Only data for $\dot{\gamma} = 4.51 \times 10^{-4}$ are shown for clarity. However, as we show in the Supporting Information the size distribution is dictated by the value of ω/β (Figure S2), just like the average size of the aggregates. From Figure 9 we conclude that under low frequency oscillatory shear the peak of the distribution moves to smaller sizes and the number of small aggregates (of approximately sizes 5−15) increases. This is consistent with the notion that the shear ruptures the aggregates. Note that the size distribution near the crossover frequency ($\omega/\beta = 5.91 \times 10^{-5}$) is still different from the unsheared one. The number of aggregates is larger as well. Only at frequencies higher than

DOI: 10.1021/acs.macromol.5b00885
Macromolecules 2015, 48, 6313−6320

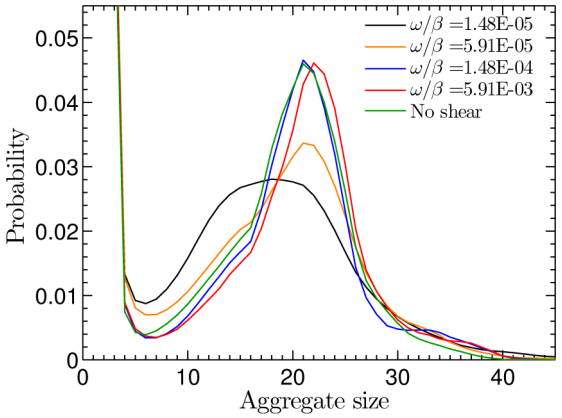

Figure 9. Probability of finding an aggregate of a given size. Data are shown for a few frequencies at shear rate of 4.51×10^{-4}.

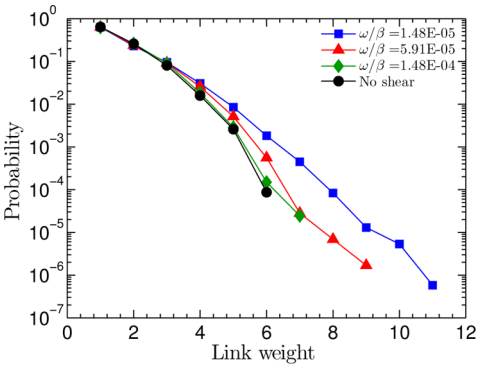

Figure 10. Probability of finding a link of a specific weight within the polymer network. Data are shown for a few amplitude and frequency combinations at a shear rate of $\dot{\gamma} = 4.51 \times 10^{-4}$.

approximately $\omega/\beta = 1.48 \times 10^{-4}$ the peak value of the distribution resembles the unsheared one. Even thought the distribution at $\omega/\beta = 5.91 \times 10^{-3}$ resembles the unsheared one, it is shifted to higher aggregate sizes. This is in agreement with Figure 8a, which shows that the number of aggregates decreases for oscillatory shear at the highest frequencies. At these frequencies the number of single sized aggregates is lower as well. This implies that the free end groups of dangling chains (Figure 7) connect to existing aggregates, thereby increasing the aggregate size. The chain beads, which surrounding every aggregate, serve as a barrier between the given aggregate and others. These beads encompass the aggregate, acting as a corona. Traversing the aggregate corona is one challenge for these free end groups. The increase in number of chains with increased aggregate size makes it difficult for two aggregates to spatially find one another. Small oscillations seem to provide a mechanism for the free end groups to pass through these corona chain beads. This leads to an association with existing aggregates and a decrease in the number of free end groups. Shear-induced aggregation has been reported on before.[23,24]

Figure 8b shows the loop to bridge ratio. Although more noisy, the data still show a clear trend. At the highest frequencies the ratio resembles that of the unsheared system. However, when the amplitude increases (frequency decreases), deviations are observed. Interestingly, the ratio peaks near the crossover frequency. This increase in the number of loops is expected since a system containing more loops is easier to shear. An increase in the loop to bridge ratio as a result of uniform shear has been anticipated and discussed previously.[26] The decrease in the ratio at even lower frequencies and larger amplitudes is surprising. We have been able to attribute this to an increase in link weight. Figure 10 shows the probability of finding a link of a specific weight for a few amplitude−frequency combinations. Compared to that of a nonsheared system the weights of the links are larger. This implies that when the system restructures so as to allow large amplitude shear, it not only forms more loops, but in addition, bridging chains that previously joined different aggregates join the same pair instead. The latter effect seems to dominate at the lowest frequencies. As the weight of links increase, this lowers the total number of links within the network. From Figure 8a, it is evident that there are more aggregates. Hence, each aggregate links to fewer others. This will make it easier for the network to deform. However, the connections that exist are on average stronger than those in the unsheared system. After all, to pull two aggregates apart which are bridged by a single weight link, a single end group would need to be freed from only one of the two aggregates. When they are bridged by multiple chains, many end groups have to be freed simultaneously. A similar transition to higher weight links was reported in a recent paper by Billen et al.[25] There it was shown under uniform shear that higher weight links tend to orient themselves parallel to the direction of shear, while the links of weight one orient perpendicular. This seems to provide a mechanism for the system to lower stresses during shearing. Only a few links containing one bridging chain have to be broken during the large amplitude oscillatory motion.

CONCLUSIONS

We utilize a molecular dynamics simulation to perform bulk rheology experiments, exploring the structural variations in a polymer network that result as a viscoelastic response. The simulation is novel in that the associative properties of the functionalized polymer end groups are modeled as reversible physical connections. This approach allows for a unique identification of which end groups are contained within a single aggregate.

The rheological properties of the simulated system are found to be consistent with experimental associative polymers. The methodology behind SRFS is used to explore the crossover between the low frequency viscous to elastic plateau regime. The network structure is shown to undergo variations throughout the viscoelastic range. A comparison with the topology of a nonsheared system gives rise to the interesting frequency dependence of these structural features. At high frequencies, small amplitude oscillations more or less preserve the network topology, although a small decrease in single-size aggregates is observed. The rapid oscillatory shear makes it possible for the singles to join existing large aggregates, making them even slightly larger. In contrast, significant topological restructuring occurs in the lower frequencies, with the onset occurring at frequencies slightly higher than the crossover. This process starts with an increase in the number of loops and a decrease in the average size of the aggregates. However, at the lowest frequencies the loop to bridge ratio decreases again. Even though more chains form bridges, the network structure is weakly connected with only a few links from each aggregate extending to others. Many of these links contain multiple chains, and we believe them to exist over long periods. Such a configuration provides a mechanism for the system to keep the need to restructure during high amplitude oscillatory shear at a

DOI: 10.1021/acs.macromol.5b00885
Macromolecules 2015, 48, 6313−6320

minimum. To confirm this picture, we plan to perform further studies on aggregate kinetics.

■ ASSOCIATED CONTENT

Supporting Information

The Supporting Information is available free of charge on the ACS Publications website at DOI: 10.1021/acs.macromol.5b00885.

A data collapse of loss moduli with the Rouse contribution subtracted out as well as the frequency dependence of the preferential size within the aggregate size distribution (PDF)

■ AUTHOR INFORMATION

Corresponding Author

*E-mail abaljon@mail.sdsu.edu (A.R.C.B.).

Notes

The authors declare no competing financial interest.

■ ACKNOWLEDGMENTS

The authors acknowledge financial supported by the National Science Foundation Grant DMR-1006980, Department of Defense DURIP Grant W911NF-10-1-0157, and the National Science Foundation Grant CHE-0947087.

■ REFERENCES

(1) Glass, J. E. Hydrophilic Polymers: Performance with Environmental Acceptability. *Advances in Chemistry Series*, 9th ed.;American Chemical Society: Washington, DC, 1996; Vol. *248*.

(2) Raafat, A. I.; Saad Eldin, A. A.; Salama, A. A.; Ali, N. S. *J. Appl. Polym. Sci.* **2013**, *128*, 1697−1705.

(3) Abandansari, H. S.; Aghaghafari, E.; Nabid, M. R.; Niknejad, H. *Polymer* **2013**, *54*, 1329−1340.

(4) Lo Verso, F.; Likos, C. N. *Polymer* **2008**, *49*, 1425−1434.

(5) Roux, R.; Ladaviére, C.; Montembault, A.; Delair, T. *Mater. Sci. Eng., C* **2013**, *33*, 997−1007.

(6) Werten, M. W. T.; Teles, H.; Moers, A. P. H. A.; Wolbert, E. J. H.; Sprakel, J.; Eggink, G.; de Wolf, F. A. *Biomacromolecules* **2009**, *10*, 1106.

(7) Ma, S. X.; Cooper, S. L. *Macromolecules* **2001**, *34*, 3294.

(8) Kujawa, P.; Watanabe, H.; Tanaka, F.; Winnik, F. M. *Eur. Phys. J. E: Soft Matter Biol. Phys.* **2005**, *17*, 129−137.

(9) Shen, W.; Kornfield, J. A.; Tirrell, D. A. *Soft Matter* **2007**, *3*, 99.

(10) Jeong, B.; Kim, S. W.; Bae, Y. H. *Adv. Drug Delivery Rev.* **2012**, *64*, 154−162.

(11) Amin, S.; Rajabnezhad, S.; Kohli, K. *Sci. Res. Essays* **2009**, *4*, 1175−1183.

(12) Baljon, A. R. C.; Flynn, D.; Krawzsenek, D. *J. Chem. Phys.* **2007**, *126*, 044907.

(13) Kremer, K.; Grest, G. S. *J. Chem. Phys.* **1990**, *92*, 5057.

(14) Allen, M. P.; Tildesley, D. J. *Computer Simulation of Liquids*; Oxford University Press: New York, 1989.

(15) Baschnagel, J.; Varnik, F. *J. Phys.: Condens. Matter* **2005**, *17*, R851.

(16) Gear, C. W. *Numerical Initial Value Problems in Ordinary Differential Equations*; Prentice Hall PTR: Upper Saddle River, NJ, 1971.

(17) Metropolis, N.; Rosenbluth, A. W.; Rosenbluth, M. N.; Teller, A. H.; Teller, E. *J. Chem. Phys.* **1953**, *21*, 1087−1092.

(18) Bedrov, D.; Smith, G. D.; Douglas, J. F. *Europhysics letters* **2002**, *59*, 384.

(19) Hyun, K.; Wilhelm, M.; Klein, C. O.; Cho, K. S.; Nam, J. G.; Ahn, K. H.; Lee, S. J.; Ewoldt, R. H.; McKinley, G. H. *Prog. Polym. Sci.* **2011**, *36*, 1697−1753.

(20) Uneyama, T.; Suzuki, S.; Watanabe, H. *Phys. Rev. E* **2012**, *86*, 031802.

(21) Doi, M.; Edwards, S. F. *The Theory of Polymer Dynamics*; Oxford University Press: New York, 1986.

(22) Wyss, H. M.; Miyazaki, K.; Mattsson, J.; Hu, Z.; Reichman, D. R.; Weitz, D. A. *Phys. Rev. Lett.* **2007**, *98*, 238303.

(23) Khalatur, P.; Khokhlov, A.; Mologin, D. A. *J. Chem. Phys.* **1998**, *109*, 9602.

(24) Tam, K. C.; Jenkins, R. D.; Winnik, M. A.; Bassett, D. R. *Macromolecules* **1998**, *31*, 4149−4159.

(25) Billen, J.; Wilson, M.; Baljon, A. R. *Chem. Phys.* **2015**, *446*, 7−12.

(26) Ganesan, V.; Fredrickson, G. H. *J. Rheol.* **2001**, *45*, 161−185.

DOI: 10.1021/acs.macromol.5b00885
Macromolecules 2015, 48, 6313−6320